The Meteoritical Society

Meteoritics & Planetary Science 57, Nr 12, 2108–2126 (2022)
doi: 10.1111/maps.13929

Analysis of the daylight fireball of July 15, 2021, leading to a meteorite fall and find near Antonin, Poland, and a description of the recovered chondrite

Lukáš SHRBENÝ[1]*, Agata M. KRZESIŃSKA[2], Jiří BOROVIČKA[1], Pavel SPURNÝ[1], Zbigniew TYMIŃSKI[3], and Kryspin KMIECIAK[4]

[1]Astronomical Institute of the Czech Academy of Sciences, Ondřejov 251 65, Czech Republic
[2]Centre for Earth Evolution and Dynamics, Department of Geosciences, University of Oslo, Oslo N-0371, Norway
[3]National Centre for Nuclear Research, POLATOM Radioisotope Centre, Otwock 05-400, Poland
[4]Meteorite Finder
*Corresponding author. E-mail: lukas.shrbeny@asu.cas.cz

(Received 04 June 2022; revision accepted 24 October 2022)

Abstract–We present the description of an observation of a fireball recorded during the sunrise on July 15, 2021. Atmospheric trajectory, impact area, and heliocentric orbit were determined on the basis of three instrumental video records. The terminal part of the fireball was not instrumentally recorded due to clouds. Based on our computations, one meteorite was found in the predicted impact area by Polish searchers. The specimen was, soon after recovery, analyzed for the presence of short-lived radionuclides and the measurement confirms a very fresh fall, coinciding with the time of the fireball event. The recovered meteorite, Antonin, is an unbrecciated L5 chondrite with shock stage S3, weathering grade W0, and bulk density of 3.42 g cm^{-3}. Unusual for L chondrites, it contains assemblages composed of metal and two sulfides, troilite and mackinawite. We interpret these assemblages to have been formed as products of shock metamorphism and post-shock annealing on the parent body. This suggests that the thermal and collisional history of the Antonin parent body was complex.

INTRODUCTION

The Czech Fireball Network is part of the European Fireball Network (EN). The main instrument on every Czech station is the Digital Autonomous Fireball Observatory (DAFO) (Spurný et al., 2017), which is supplemented by its spectral equivalent (SDAFO) (Borovička et al., 2019) at some stations. These photographic cameras provide us with precise records of fireballs, but observations are only made at night and also during the darker parts of dusk and dawn. In order to cover the entire twilight periods, as well as the rest of the day, we supplemented DAFO and SDAFO by a set of security internet protocol (IP) video cameras on two Czech stations (Ondřejov in 2017 and Kunžak in 2018) to cover the whole sky. The main purpose of these IP cameras is to record the fragmentation of fireballs. The vast majority of the stations are also equipped with a surveillance IP camera to inspect the condition of DAFO. For more details, see Shrbený et al. (2020). These supplementary IP cameras have already recorded several fireballs at a time when DAFOs do not take pictures because of the light. The most important daylight record was the observation of a very bright bolide connected with a probable meteorite fall on April 4, 2020 (EN060420_133330), which was recorded from three stations (the impact area is located east of Berchtesgaden on both sides of the German–Austrian border; so far, no meteorite has been recovered).

In general, using video cameras is the only way to optically record fireballs also in daylight. There are a couple of video camera networks observing meteors, but in the case of light-sensitive (hardware limitation) cameras, these can observe only at night. Daylight observations may also be limited by software issues, as is the case of the Fireball Recovery and InterPlanetary Observation Network (FRIPON). Their reduction pipeline provides a high false-positive detection rate at the moment, but a new version is being developed so that daytime observations should become possible (Colas et al., 2020).

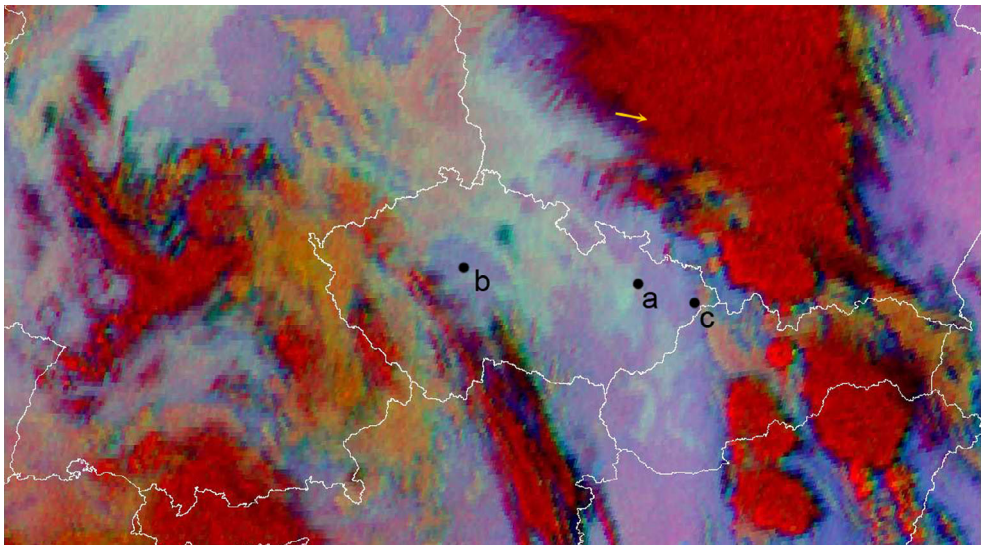

Fig. 1. Satellite image of Central Europe taken on July 15, 2021 at 3 UT by Metosat geostationary meteorological satellite (courtesy EUMETSAT and Czech Hydrometeorological Institute). Projection of observed part of the atmospheric trajectory of the fireball (orange arrow) and locations of the three video camera stations used for the trajectory determination (black dots) Červená hora (a), Říčany (b), and Lysá hora (c) are also shown. The meaning of the colors in the picture: red shows vertically massive clouds, dark blue shows sparse cirrus clouds, medium and low clouds are ochre, the lowest clouds and fog are turning green, and pink shows the surface. (Color figure can be viewed at wileyonlinelibrary.com.)

In the case of dedicated video meteor observation, we have to mention the Allsky7 Fireball Network in Europe and United States (Hankey et al., 2020), both equipped with the same hardware and software. The observatories consist of seven individual IP cameras covering the whole sky and recording bright meteor events also in daylight. One station of this network recorded part of the fireball preceding the Flensburg meteorite fall in 2019 in Germany (Borovička et al., 2021).

Three of our IP cameras recorded a daylight fireball on July 15, 2021 during a sunrise. From the position of the IP cameras and their orientation, it was obvious that the fireball flew north of the Czech Republic. As it turned out, from our records, it was possible to describe all the basic parameters of the fireball. In the following sections, we will describe the fireball observations, trajectory, fragmentation, and heliocentric orbit, as well as the meteorite recovery, measurement of cosmogenic radionuclides and petrographic characterization, mineral composition, and shock properties which, altogether, allow us to address questions of meteorite parent body history and meteoroid size.

OBSERVATIONS

On July 15, 2021, Thursday, we received a total of eight reports via our web form of sightings of a bright fireball visible at approximately 3 UT that day. There had been thunderstorms in many places the night before, and even in the morning, many places were covered with clouds or morning fog had formed (Fig. 1). However, it cleared up in some places and the fireball could be seen. The sky was already bright as the Sun was just rising. The photographic cameras of our fireball network were no longer working for this reason, but this was not the case for our video cameras. The fireball was recorded by IP video cameras at the stations Červená hora and Lysá hora in the Moravian–Silesian region and at Říčany near Prague (Fig. 1). From these three recordings, we reconstructed the atmospheric trajectory and velocity of the fireball. It turned out that the fireball (when observed from a standard distance of 100 km) reached at least the brightness of the full Moon and penetrated deep into the atmosphere, suggesting that a meteorite impact on the Earth's surface occurred. Unfortunately, the final part of the luminous flight of the bolide was not recorded by the cameras, as the bolide flew behind the clouds at Červená hora (see Fig. 2a), it was out of the field of view (FOV) at Říčany (Fig. 2b), and only a small part of the bolide was recorded in the gap between the clouds at Lysá hora (Fig. 2c).

The exact type of camera, the resolution, FOV, frame rate, limiting magnitude, and geographic coordinates of all cameras are listed in Table 1. Four megapixel-wide FOV IP cameras of the same type were in operation on Červená hora and Lysá hora and a

Fig. 2. Composition images of details of recorded parts of the atmospheric trajectory of the EN150721_030011 bolide. The order of images corresponds to description in caption of Fig. 1. (Color figure can be viewed at wileyonlinelibrary.com.)

Table 1. Detailed information about the IP cameras that recorded the bolide.

	Červená hora	Lysá hora	Říčany
Manufacturer	Dahua	Dahua	Dahua
Type of camera	IPC-HFW4431EP	IPC-HFW4431EP	IPC-HFW5442EP
Resolution (pix)	2688 × 1520	2688 × 1520	2688 × 1520
Horizontal FOV (°)	83	83	56
fps	25	25	25
LSM@25fps (mag)	4	4	6.5
Geographical coordinates	49.7773, 17.5420	49.5464, 18.4476	49.9926, 14.6832

FOV = field of view; fps = frames per second; LSM = limiting visual stellar magnitude in the center of FOV.

more sensitive IP camera with medium FOV was operated in Říčany. All our IP cameras record continuously on a memory card and the oldest recordings are automatically overwritten after a few days. Each meteor record must be calibrated using stars recorded by the same camera. Even though the IP cameras are fixed on the stations, our experience shows that the position of the camera changes slightly over time. This leads to the conclusion that only stars temporally close to the passage of a given meteor should be used for record reduction. In general, stars older than 1 month are unsuitable for reduction and bring a systematic error in the atmospheric trajectory solution. In the case of this fireball, we manually changed the exposure time remotely (one-third of a second is the maximum value of our IP cameras) at several times during the night after the event to get a sufficient number of reduction stars in the FOV of the IP cameras at Červená hora and Lysá hora. These records were combined with stars recorded in days before the fireball. Stars recorded only 2 h before the fireball were used for calibration of more sensitive IP camera at Říčany. All records were measured manually by FishScan software and calculations were done by Boltrack software, both written by Jiří Borovička. The methods and procedures used in these software packages are described in Borovička et al. (2022).

For completeness, we add that one of the witnesses filmed the bolide with a dashboard camera, but even in this footage, the end of the luminous path of the bolide is obscured by clouds. We thus have no information about the size and number of possible meteorites, because it is not clear whether and into how large pieces the object broke up at the end of its trajectory.

We tried to get a record of this fireball from Germany or Poland, but no other record or observation could be found. The meteor has not been observed anywhere else than the Czech Republic. Without the reports of the above-mentioned casual witnesses, this meteorite fall would have gone unnoticed.

Table 2. Parameters of the atmospheric trajectory of the EN150721_030011 bolide.

	h (km)	Lat. (°)	Long. (°)	v (km s^{-1})	z_R (°)	L (km)	p_{dyn} (MPa)
beg	73.92	51.5852	17.2927	17.68 ± 0.01	37.45	0	0.015 ± 0.001
last	24.96	51.5094	17.8178	13.2 ± 0.3	37.69	61.8	7.0 ± 0.3

Parameters are given for the observed beginning (beg) and the last observed point (last) as follows: h is height, Lat. and Long. are geographical latitude and longitude, v is observed atmospheric velocity, z_R is zenith distance of the radiant, L is length of the trajectory, and p_{dyn} is dynamic pressure.

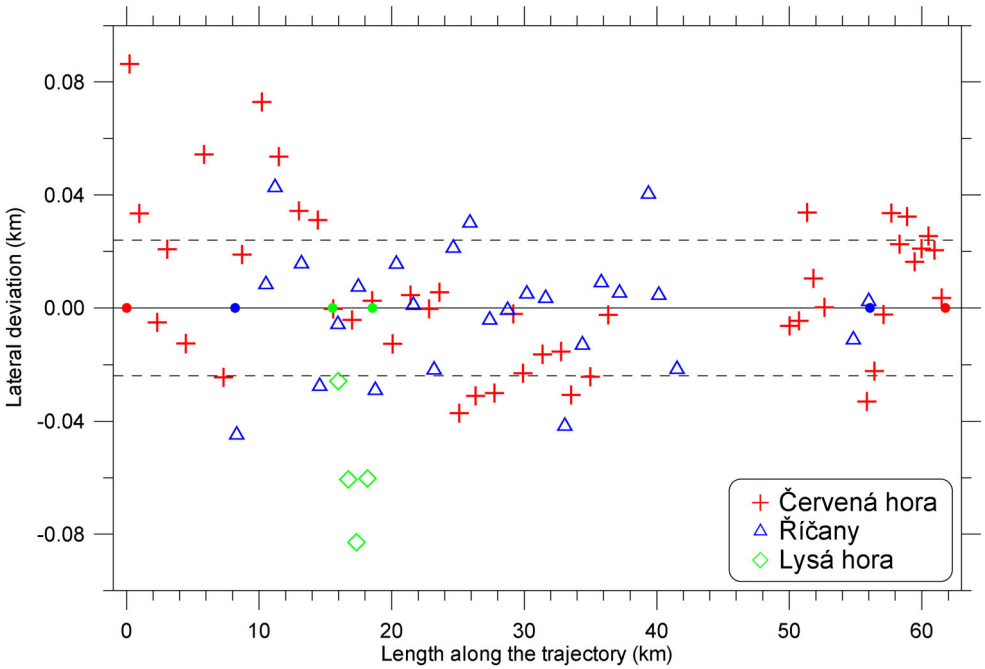

Fig. 3. Lateral deviation of measured points along the atmospheric trajectory. Small color dots mark the first and the last observed points from individual stations. Dashed lines show the range of one standard deviation of 23 m. Note the different scales on the x- and y-axes. (Color figure can be viewed at wileyonlinelibrary.com.)

ATMOSPHERIC TRAJECTORY AND HELIOCENTRIC ORBIT

The basic parameters of the atmospheric trajectory of the EN150721_030011 bolide are presented in Table 2. The trajectory was determined on the basis of three video records and any point on the trajectory has standard deviation of 23 m. Lateral deviation of measured points along the atmospheric trajectory is presented in Fig. 3.

Atmospheric Trajectory

The whole event took place over the territory of Poland at a distance of about 130 km from the Czech border (Fig. 2). The fireball was first detected at 3:00:11 UT at an altitude of 73.9 km at 17.7 km s^{-1} with an angle of 52.4° to the surface. The last detection was at an altitude of 25.0 km and the fireball still had a velocity of about 13 km s^{-1}. A detailed projection of the recorded luminous trajectory of the bolide onto the Earth's surface is shown in Fig. 4. The computed initial velocity is 17.74 ± 0.02 km s^{-1}. The fireball lasted 3.64 s on the three records and the observed length of the atmospheric trajectory was 61.8 km. The initial dynamic mass of the meteoroid is estimated to be between 50 and 100 kg, which corresponds to a sphere with a radius of about 15–20 cm (for a density 3.5 g cm^{-3}). The terminal mass is unknown, but the dynamic mass at the last observed part of the trajectory is of the order of few tens of kilograms. The expected meteorite fall occurred south of the town of Mikstat (Fig. 5).

The photometry of the fireball was measured at the Červená hora record and was calibrated by the Moon recorded by the same type of video cameras at four Czech stations in the evenings from 12 to 15 July at times when the altitude of the Sun corresponds to the altitude of the Sun during the fireball passage. This way, the value of the camera's gain, which is changed

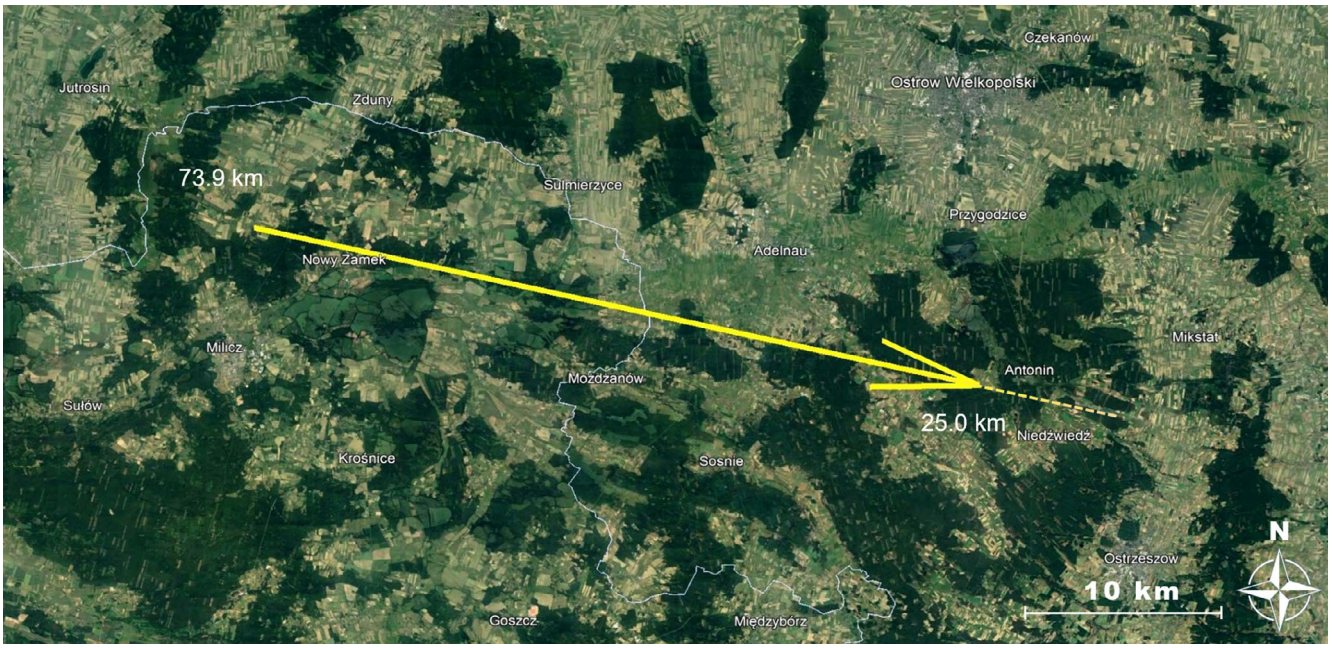

Fig. 4. Projection of the recorded luminous trajectory of the bolide onto the Earth's surface. (Color figure can be viewed at wileyonlinelibrary.com.)

Fig. 5. Impact area of EN150721_030011. The position of the recovered meteorite is marked with a red circle. The town of Antonin is located just beyond the left edge of the image. (Color figure can be viewed at wileyonlinelibrary.com.)

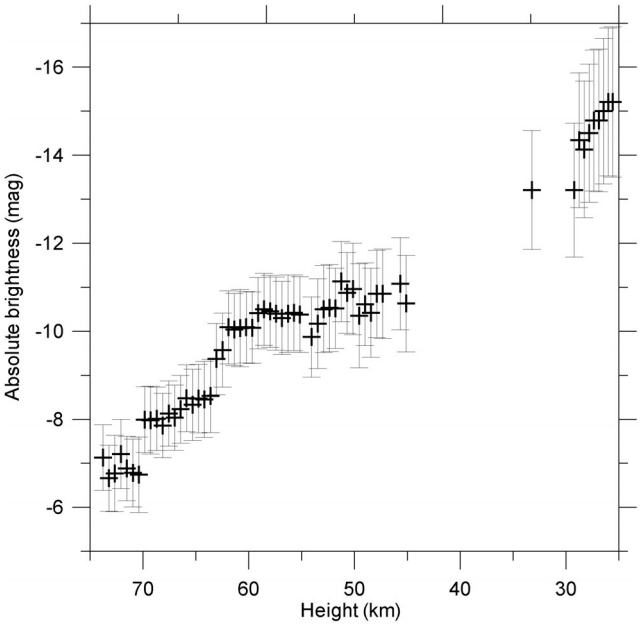

Fig. 6. Light curve of the Antonin bolide as measured at the Červená hora record.

automatically during the twilight, was approximated. Owing to the fact that the FOV center of our IP cameras is not in the same elevation above the horizon, this difference for each station was converted to the FOV of the camera at Červená hora. Dark image and flat field were also taken into account. The resulting photometry during the daylight has relatively large uncertainties (up to 1.7 magnitude at the maximum brightness) and should be considered approximative. The fireball was first detected having the absolute brightness of approximately −7 mag and the maximum observed absolute brightness of −15 mag was reached at an altitude of 25 km, just before it disappeared behind the clouds (Fig. 6). The sharp increase in brightness was observed at an altitude of 63 km, which corresponds to the maximum observed wake length. For these luminosities, the initial meteoroid mass would be about 200 kg, but due to large errors, it can be in the range of 50–500 kg. The luminous efficiency was taken from Revelle and Ceplecha (2001) for 10 kg mass of the meteoroid. The dynamic mass is smaller, but compatible within the measurement errors.

Appearance of the Fireball and Probable Fragmentation Points

The fireball is best seen at station Červená hora. The bolide flew down to an altitude of 66 km as a point-like object and then a faint wake appeared, which corresponds to the first observed fragmentation of the meteoroid. The dynamic pressure ($p = \rho v^2$) at this point is 0.044 MPa and corresponds to typical dynamic pressures of first fragmentation phase of ordinary chondritic material (Borovička et al., 2020). The wake reached a maximum length of about 1.5 km at altitudes between 63 and 62 km. The wake disappeared just below 55 km and a very faint and short wake appeared again at 51 km. The same appearance is visible also from Říčany. Only a small part of the trajectory at altitudes between 62 and 59 km is visible from Lysá hora. The fireball is behind clouds at altitudes between 45–34 and 33–30 km at station Červená hora and at altitudes between 44 and 33 km at station Říčany. At the end of the footage from Říčany, the bolide passes behind a tree and its shape is thus affected and these data points cannot be used to determine the velocity but only the trajectory. At that time, it was at altitudes between 33 and 29 km. The fireball fragmented again probably at altitudes between 45 and 34 km, when it was obscured by clouds. Just before the cloud, as visible from Červená hora, the wake was very faint and short, but just after the cloud, the wake was bright and long. The dynamic pressure ranges between 0.6 and 2.5 MPa, as the fireball passes behind the cloud, with mean value of 1.1 MPa for the altitude of 40 km and velocity of 17 km s^{-1}. Also these dynamic pressures correspond to the second stage of fragmentation described by Borovička et al. (2020). We assume that several macroscopic fragments were formed during this fragmentation at around 40 km, which is also confirmed by the Červená hora record. Two fragments can be seen separated from the rest of the wake on a couple of video frames. At that time, the fragments were at altitudes between 28 and 26 km. We do not know what happened with the fireball below 25 km, since there is no record available for this terminal part of the trajectory. The dynamic pressure at the last observed point is 7.0 ± 0.3 MPa. Both scenarios are still possible: with another fragmentation and without fragmentation. The high-altitude wind data for calculation of the dark flight and location of the impact area were kindly provided by the Czech Hydrometeorological Institute. If a large meteorite of about 10 kg survived the descent, it is located in the eastern part of the impact area. If it broke up into smaller fragments with masses around 100 grams, these fell about 7 km farther to the west (Fig. 5).

Heliocentric Orbit

The geocentric radiant and orbital elements of the EN150721_030011 Antonin were computed by the analytical method of Ceplecha (1987) and are presented in Table 3. Before the collision with the Earth, the meteoroid orbited the Sun in an elliptical orbit with small semimajor axis (1.13 AU) and eccentricity (0.23), but with a relatively large inclination of 24 degrees to

Table 3. Geocentric radiant and heliocentric orbit of the EN150721_030011 (J2000.0).

Geocentric radiant and velocity	
Right ascension (°)	292.32 ± 0.03
Declination (°)	41.64 ± 0.04
Velocity (km s^{-1})	14.04 ± 0.03
Heliocentric orbit	
Semimajor axis (AU)	1.1269 ± 0.0007
Eccentricity	0.2285 ± 0.0006
Perihelion distance (AU)	0.8694 ± 0.0003
Argument of perihelion (°)	257.16 ± 0.09
Ascending node (°)	112.5807 ± 0.0001
Inclination (°)	24.22 ± 0.05
Tisserand parameter	5.443 ± 0.003
Time of perihelion (day)	2020 Jul 7.2 ± 0.5
Orbital period (year)	1.1963 ± 0.0011

the orbital plane of the planets (Fig. 7). On the basis of its Tisserand parameter, it was orbiting the Sun on an asteroidal orbit.

METEORITE RECOVERY AND HAND SPECIMEN DESCRIPTION

A few days after the fall, when all important parameters of the fireball were determined, the Czech part of the team published the basic information and the impact area on their website www.asu.cas.cz/~meteor/bolid/ and informed colleagues and searchers in Poland. Several dedicated recovery expeditions were performed by private people and organized groups. During one of the attempts, on August 3, 2021, one piece of meteorite was recovered on the field road site on WGS84 coordinates of 51.5135° N, 17.9047° E by Kryspin Kmieciak, in the predicted fall location for a corresponding mass and information about the find was published on the cosmoartel.pl and woreczko.pl servers and by Owczarzak (2021). The specimen was 352 g in mass, almost fully covered by thick fusion crust (Fig. 8). It was covered with mud and had some vegetation traces attached to the surface. Although humid on the surface, the specimen was visibly fresh and intact of weathering. Of note is that, within the first month after recovery, it lost some mass (down to 350 g) due to dewatering and drying. Similar behavior was documented also for meteorite Žďár nad Sázavou the specimen M2, which lost almost 2 g in the first 2 days after the recovery (Kalasová et al., 2020; Spurný et al., 2020). There is no other recovered meteorite known to us from this fall by now. A long and intensive search was carried out in the impact area and no other meteorite fragments were found. This may mean that the large mass of the body observed at the last point did not break up significantly afterwards. Then, there would be one large, still unfound, piece of meteorite in the eastern part of the impact area (see section Appearance of the Fireball and Probable Fragmentation Points).

CHARACTERIZATION OF THE RECOVERED SPECIMEN

Analytical Methods—Cosmogenic Radionuclides

The recovered meteorite (before any subsampling) was tested for the presence of short-lived radionuclides to determine the time of its fall and verify its connection to the fireball event. The whole meteorite investigation was conducted with nondestructive methods at the gamma-ray spectrometry laboratory at the National Centre for Nuclear Research in Poland. Two series of measurements were carried out 28 days after the meteorite fall and the results confirmed that the Antonin meteorite did not come from a fall older than 30 days.

A high purity germanium (HPGe) detector with a relative efficiency of 45% (energy 1332.5 keV of ^{60}Co) and an energy resolution full width at half maximum of 2.0 keV was used for the analyses. In order to reduce the background radiation, the spectrometer was placed in a lead chamber lined with copper plates. The whole specimen was measured in close proximity to the detector endcap. Description of measurement methods and applied 3-D scanning techniques to Monte Carlo calibration and the coincidence summing correction can be found in Tymiński et al. (2022). Total measurement time lasted for 177 h. The measurement methods of Tymiński et al. (2022) ensured the efficiency calibration contribution to the overall measurement uncertainty to remain <3.0% (1 sigma). The total activity uncertainty was imposed mainly by counting statistics. The standard components of the uncertainty were dominated by the statistics of counts in the measured spectra and the Monte Carlo efficiency calculations, where the main unknown is the precision of the detector geometry and the meteorite homogeneity in terms of radionuclide concentration and density (self-attenuation). A significant component of the uncertainty was also the uncertainty of the gamma ray coincidence summing correction. Apart from the standard components of uncertainty, the changes in the mass of the specimen during the measurement (352 g immediately after recovery, 350 g after the isotopic measurement) were taken into account. Since drying the meteorite would take time, the meteorite was not intentionally dried before cosmogenic radionuclide measurements. This was done to ensure that very short-lived species such as ^{48}V and ^{51}Cr were at quantifiable levels.

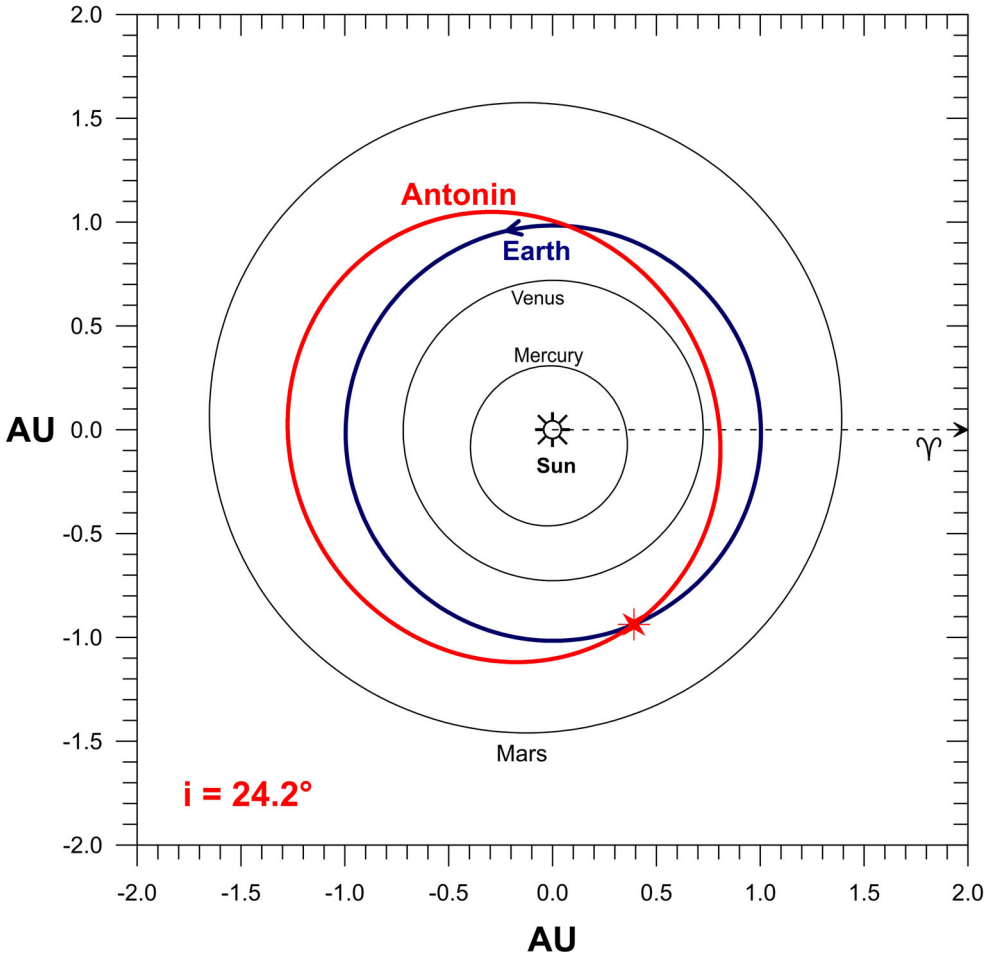

Fig. 7. Heliocentric orbit of the EN150721_030011 Antonin projected onto the ecliptic plane. (Color figure can be viewed at wileyonlinelibrary.com.)

Analytical Methods—Petrographic Characterization of the Sample and Bulk Density

Several slices were cut off from the recovered specimen. One of them (~3 cm × 2 cm) was utilized to prepare a thin section, which was explored for classification. Texture of meteorite was characterized with optical light microscopy as well as scanning electron microscopy, and the chemical composition of various minerals was determined with electron microprobe. Backscattered electron (BSE) microscope images and energy-dispersive X-ray (EDX) maps were collected with Hitachi SU5000 FEG-SEM (Schottky FEG) equipped with Dual Bruker Quantax Xflash 30 EDS system, at the Department of Geosciences, University of Oslo. The instrument was operating at 15 kV and 11 mm working distance. EDX maps were acquired with magnification of 50–100 times, spatial resolution (pixel size) of 1.0–1.4 μm, and acquisition time of at least 1.0 ms per pixel.

Electron microprobe measurements were performed with a Cameca SX-100 at the Department of Geosciences, University of Oslo. Beam current was set on 20 nA (10 nA for glassy phases) and accelerating voltage on 15 kV. Analyses were conducted with 1 μm, focused electron beam for most minerals, apart from phosphates and glasses for which defocused 5–10 μm-sized beam was applied. Counting times up to 10–20 s per element were applied to analyze major and selected minor elements. For the presence of Co and Cu in iron–nickel metal alloy, counting time of 40 s was applied. Natural and synthetic standards were used to transform count rates into element concentrations and procedure of PAP correction (Pouchou & Pichoir, 1991) was applied to correct peak overlaps. An additional correction was applied to remove interference of the Fe-Kβ peak on the Co-Kα peak in iron–nickel metal phases.

Bulk composition of meteorite was calculated by combining modal mineral composition retrieved from EDX mappings and chemical composition of minerals obtained by electron probe microanalysis (EPMA). Modal mineral composition was calculated in ImageJ (Schneider et al., 2012), by reprocessing elemental EDX

Fig. 8. Recovered 352 g specimen in situ. (Color figure can be viewed at wileyonlinelibrary.com.)

montages collected at 70× magnification. To obtain mean bulk chemical composition, average composition of minerals (as determined by EPMA) within mapped area was implemented into modal composition.

The bulk density of the specimen was calculated based on the mass to volume ratio. Volume was obtained from a 3-D scanning visualization that was reconstructed during efficiency calculations for cosmogenic radionuclide analysis (for method details, see Tymiński et al., 2022). The volume is 102.2 cm^3 with relative error of 0.15%. The sample had not been dried at approximately 100 °C for several hours, so there still was uncertainty in the amount of water that was left in the specimen. We assumed that it was at least as much as has already been evaporated. The relative error of mass is therefore 0.6%. For the mass of 350 g, the bulk density is 3.42 ± 0.02 g cm^{-3}. This value corresponds to mean bulk density 3.40 ± 0.15 g cm^{-3} of L chondrites (Wilkinson & Robinson, 2000).

Petrography of Antonin and Composition of Minerals

The petrography of the meteorite corresponds to an ordinary chondrite, composed predominantly of olivine, low-Ca orthopyroxene, troilite, kamacite, and taenite. Accessory minerals include chromite, ilmenite, merrillite, and Cl-apatite. Under microscope, many retained and well-delineated chondrules are seen (Fig. 9a and 9b). Their mesostasis is composed of feldspathic glass with diopside microcrystallites (Fig. 9a and 9b). Crystalline plagioclase is rare, and, if present, the crystals are smaller than 50 μm.

Despite low degree of textural equilibration, minerals are chemically very homogeneous. EPMA results indicate well-equilibrated olivine with Fa content in range of 23.9–25.1 mole%, 0.41–0.55 wt% of MnO, and CaO content up to 0.07 wt% (Table 4). Orthopyroxene is also well equilibrated and shows the range of composition of 20.4–21.9 mole% Fs and 0.7–2.0 mole% Wo across the thin section. Minor contribution of MnO (0.45–0.57 wt%), Cr_2O_3 (up to 0.33 wt%), and Al_2O_3 (0.04–0.51 wt%) is detected in pyroxene. Rare plagioclase crystals have 6.9–9.0 mole% An and 5.3–7.9 mole% Or, and up to 0.84 wt % FeO (Table 4). The retained feldspathic glass shows wide range of compositions with up to 30 mole% An and 2.9–15.5 mole% Or, and up to 1.6 wt% FeO. Submicron-sized diopside crystallites in glass reveal 8.4 mole% Fs (6.3–11.6) and 46.1 mole% Wo (44.8–48.3).

Among opaque minerals, the major one is taenite with 33.4 wt% Ni (29.9–36.5 wt%) and 0.22 wt% Co (0.12–0.45 wt%). Kamacite has 6.63 wt% Ni (6.1–7.1wt % Ni) and 0.72 wt% Co (0.49–0.85 wt%, Table 5). No tetrataenite was identified.

Chromite is well equilibrated and dominated by Fe and Cr (Fe/[Fe + Mg] in range of 0.86–0.89 and Cr/[Cr + Al] in range of 0.81–0.87). It contains trace

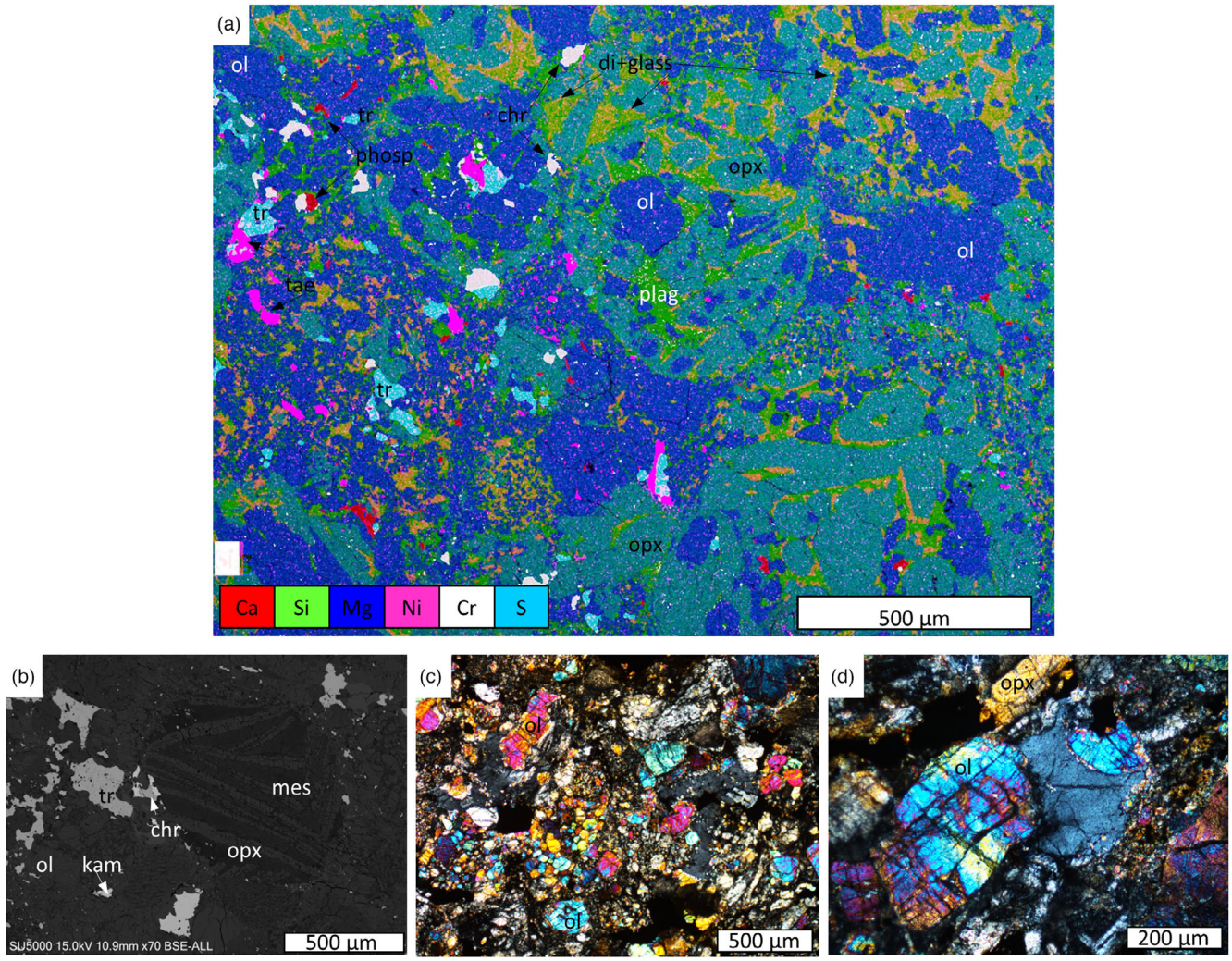

Fig. 9. Chondritic texture of Antonin meteorite, with well-delineated chondrules visible and retained feldspathic mesostasis and diopside crystallites. a) EDX elemental composite map. Dark blue is olivine (ol), light blue—low-Ca pyroxene (opx), green—plagioclase (plag) or feldspathic glass, yellow is diopside (di). Accessory phases are troilite (tr, cyan), taenite (tae, purple) or kamacite (kam), chromite (chr, white), and phosphates (phosp, red). b) BSE image of chondrule. c) Optical micrograph under cross-polarized light, showing delineated chondrules, fine-grained matrix, and weakly or moderately deformed olivine crystals. d) Olivine crystals in higher magnification showing undulose extinction of polarized light and set of planar fractures. (Color figure can be viewed at wileyonlinelibrary.com.)

amounts of TiO_2 (1.3–2.5 wt%), MnO (0.6–0.8 wt%), V_2O_3 (0.6–0.8 wt%), and ZnO (0.2–0.4 wt%). Two grains of ilmenite were found, and they are also dominated by Fe, with geikielite (Mg-ilmenite endmember) content in range 10.4–13.3 mole% and pyrophanite (Mn endmember) being 3.0–3.2 mole%. Among phosphates, both Cl-apatite and merrillite are present. Cl-apatite contains up to 5.1 wt% Cl and minor amount of Na_2O (up to 0.35 wt%). Merrillite is dominated by Ca, but up to 2.8 wt% of Na_2O and 0.8 wt% FeO were detected in it. Sulfides are represented by stoichiometric troilite and mackinawite, which is most likely a product of shock metamorphism and discussed later.

Modal mineralogy, as calculated from EDX pixel counting and bulk chemical composition retrieved from modal abundance of minerals and their chemical composition are shown in Table 6.

The meteorite is apparently weakly to moderately shocked and unbrecciated. Olivine crystals reveal undulose extinction of light and minor planar fracturing (Fig. 9c and 9d). However, many textural features are present suggesting local shock melting at contacts of minerals of contrasting densities. Shock melt pockets, a few hundred micrometers in size, are very abundant at contacts of metal and plagioclase or troilite and plagioclase (Fig. 10a). They are composed of silicate glasses and globular metal or metal–troilite assemblages

Table 4. Chemical composition of silicate minerals as determined by EPMA.

wt%	Olivine				Low-Ca pyroxene			Diopside		Plagioclase	
Al_2O_3	n.a.	n.a.	n.a.		0.08	0.10	0.21	1.67		20.77	20.24
MgO	38.17	38.79	38.39		28.90	28.74	28.88	16.07		0.01	0.03
SiO_2	38.45	38.40	38.22		55.76	55.64	55.35	55.06		66.40	66.34
TiO_2	0.12	b.d.	0.03		0.07	0.11	0.28	0.33		n.a.	n.a.
CaO	0.03	b.d.	b.d.		0.56	0.69	0.67	21.33		1.74	1.50
FeO	22.39	22.40	21.98		13.66	13.72	13.65	4.38		0.47	0.84
MnO	0.50	0.53	0.51		0.49	0.46	0.49	0.16		n.a.	n.a.
Cr_2O_3	0.10	b.d.	b.d.		0.08	0.09	0.13	0.69		n.a.	n.a.
Na_2O	n.a.	n.a.	n.a.		b.d.	0.03	b.d.	1.26		10.32	9.99
K_2O	n.a.	n.a.	n.a.		b.d.	b.d.	0.02	0.02		1.11	1.41
Total	99.80	100.13	99.14		99.61	99.57	99.69	100.97		100.83	100.36
Fo mole%	74.82	75.09	75.26	En	78.18	77.82	78.01	47.47	Ab	85.89	85.05
Fa mole%	24.62	24.33	24.17	Fs	20.72	20.84	20.68	7.25	Or	6.10	7.87
Tp mole%	0.56	0.58	0.57	Wo	1.10	1.34	1.31	45.28	An	8.00	7.08

b.d. = below detection limit, n.a. = not analyzed.

Table 5. Chemical composition of iron–nickel and sulfides as determined by EPMA.

	Kamacite			Taenite			Troilite		Mosaic troilite		Mackinawite	
Fe	93.22	91.97	93.03	65.07	69.10	64.68	63.06	62.41	62.50	62.51	48.12	48.78
Ni	6.11	7.04	6.66	33.66	29.93	35.34	b.d.	0.11	0.19	0.54	16.70	16.72
Co	0.77	0.71	0.82	0.25	0.21	0.16	0.07	0.07	0.10	0.04	0.08	0.06
Cu	b.d.	0.02	b.d.	0.17	0.17	0.14	0.04	0.03	0.10	0.08	0.86	0.61
S							37.18	37.31	36.67	37.10	34.12	33.90
Total	100.10	99.74	100.50	99.15	99.40	100.32	100.35	99.93	99.56	100.27	99.88	100.07
Fe							0.97	0.96	0.98	0.97	0.81	0.83
Ni							0.00	0.00	0.00	0.01	0.27	0.27
S							1.00	1.00	1.00	1.00	1.00	1.00

b.d. = below detection limit.

Table 6. Modal mineralogy and bulk chemical composition of Antonin meteorite as calculated from thin section by combining pixel counting on EDX mineral maps and EPMA point analyses.

Mineral	ol	opx	di	fsp and glass		phos	chr	tr	kam	tae				
vol%	43.3	32.5	5.5	9.3		0.5	0.1	5.9	1.4	1.4				
Element	Si	Ca	Ti	Fe	Mg	Mn	Ni	Cr	O	P	Na	K	Al	S
wt%	19.37	1.27	0.06	21.25	14.84	0.29	1.10	0.50	36.69	0.10	0.59	0.07	0.83	2.84

with varying proportions of glass to globules from one melt pocket to another. Chromite–plagioclase assemblages (CPA) are also present (Fig. 10b).

Many metal grains show structure of plessitic intergrowths, with taenitic domains having Ni content of 25–35 wt%. The majority of the troilite grains are visibly porous. Unusual for an ordinary chondrite, metal–sulfide assemblages are quite abundant. They are composed of patchy sulfide, in which Ni-rich and Ni-poor domains are present (Fig. 10c). The sulfide grains look mosaic, polycrystalline under optical microscope, and further investigation shows that they are composed of 10–20 μm-sized domains of mixed mackinawite and troilite (Fig. 10c). Troilite parts of mosaic aggregates are compositionally similar to bulk rock troilite, having up to 0.5 wt% Ni and trace amount of Co and Cu (Fig. 10; Table 6) and have stoichiometry of pyrrhotite with formula Fe_{1-x} S (where x = 0.03–0.04). Mackinawite has correct stoichiometry and shows formula of $(Fe,Ni)_{1+x}S$, where x = 0.08–0.10. Within the domains, small crystallites of Ni-poor kamacite are present close to contacts with metal (Figs. 10c and 11). In some places, sulfides are present within kamacite or plessite, for which Ni content is intermediate between troilite and mackinawite (Fig. 11).

Cosmogenic Radionuclides

The presence of 12 short- and medium-lived radionuclides was identified in the sample (Table 7). The distinct cosmogenic isotopes were detected at the uncertainty level of the range of 6–8% (^{22}Na, ^{26}Al, ^{46}Sc

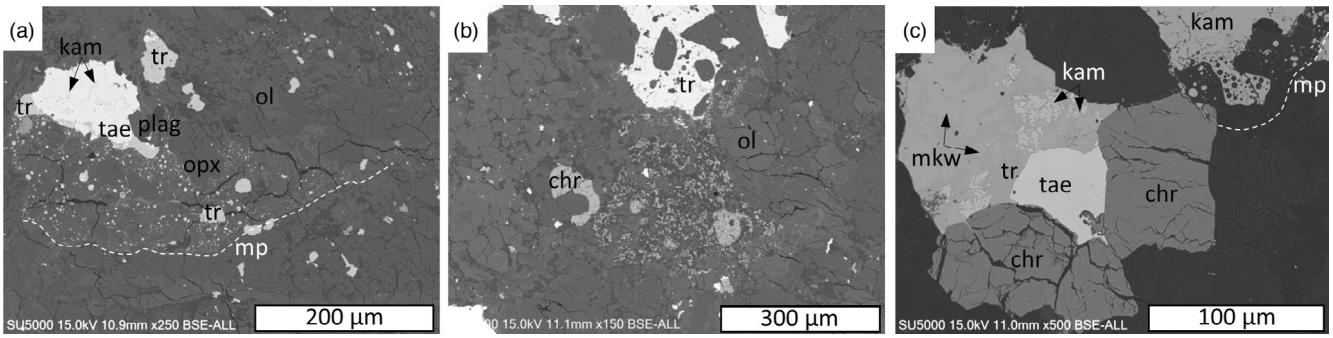

Fig. 10. Shock features in Antonin meteorite. a) Melt pocket (mp) developed at contact of metal and plagioclase and plessitic intergrowth of kamacite and taenite. b) Chromite–plagioclase assemblage. c) Patchy troilite grain with mackinawite (mkw) domains and Fe,Ni intergrowths. BSE images, mineral abbreviations as in Fig. 9.

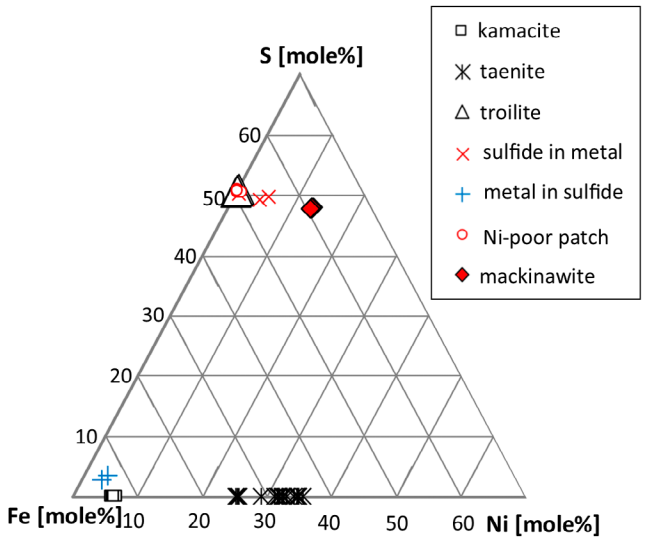

Fig. 11. Composition of metal and sulfide minerals in ternary Fe-Ni-S space. (Color figure can be viewed at wileyonlinelibrary.com.)

and ^{54}Mn, ^{57}Co, ^{58}Co, respectively) and up to 14% (^{7}Be, ^{60}Co, ^{56}Co). From this group of isotopes, ^{7}Be is distinguished, since the measured activity of 147 dpm kg^{-1} is high. The observed range of ^{7}Be in ordinary chondrites is 30–210 dpm kg^{-1} (Povinec et al., 2015), but typical values of 30–125 dpm kg^{-1} are expected from the variations of the solar cycle (Laubenstein et al., 2012).

Traces of the radionuclides with the shortest half-life: ^{48}V (15.97 days of half-life) and ^{51}Cr (27.70 days) were detected in the sample. Detection of ^{48}V had high uncertainty (70%) at very low count rate (3.8 e-5 per second), yet is clearly distinctive from the background. The gamma-emitting ^{51}Cr was relatively distinctive in the spectra (count rate 7.5 e-5 per second) and its measurement uncertainty was about 25%. Both radionuclides confirm that the meteorite is very fresh and has terrestrial age roughly 1 month before the time of analysis.

Table 7. Cosmogenic radionuclide activity in 350 g meteorite specimen (before subsampling).

Nuclide	Half-life	Radioactivity dpm kg^{-1} (±2 sigma)
^{7}Be	53.22 yr	147 (16)
^{22}Na	2.603 yr	78.6 (4.9)
^{26}Al	717 kyr	49.3 (3.3)
^{44}Ti	60.0 yr	1.12 (0.25)
^{46}Sc	83.79 days	12.4 (0.9)
^{48}V	15.97 days	Detected, ~10.9 (7.6)
^{51}Cr	27.70 days	84 (27)
^{54}Mn	312.2 days	74.0 (4.5)
^{56}Co	77.24 days	6.10 (0.79)
^{57}Co	271.8 days	7.17 (0.58)
^{58}Co	70.85 days	12.0 (1.0)
^{60}Co	5.27 yr	3.43 (0.55)

dpm kg^{-1} = decay per minute per kilogram.

DISCUSSION

Classification

The Antonin meteorite is an equilibrated ordinary chondrite. The composition of olivine and pyroxene, as well as the elemental composition of olivine and kamacite (Fig. 12) indicates that it matches well the composition of equilibrated L chondrites (Brearley & Jones, 1998; Rubin, 1990). This is confirmed by its modal and bulk chemistry (Table 6) that fits in well with the mean composition of this group (Hutchison [2004] and references therein). Based on very homogeneous composition of olivine (spread of 1.2 mole% Fa across whole analyzed section, 23.9–25.1 mole% Fa) and low-Ca pyroxene (spread of 1.5 mole% Fs, 20.4–21.9 mole% Fs), the Antonin is classified as type L5 chondrite. However, texturally the sample shows some heterogeneity and in places feldspathic glass or very fine-grained plagioclase is

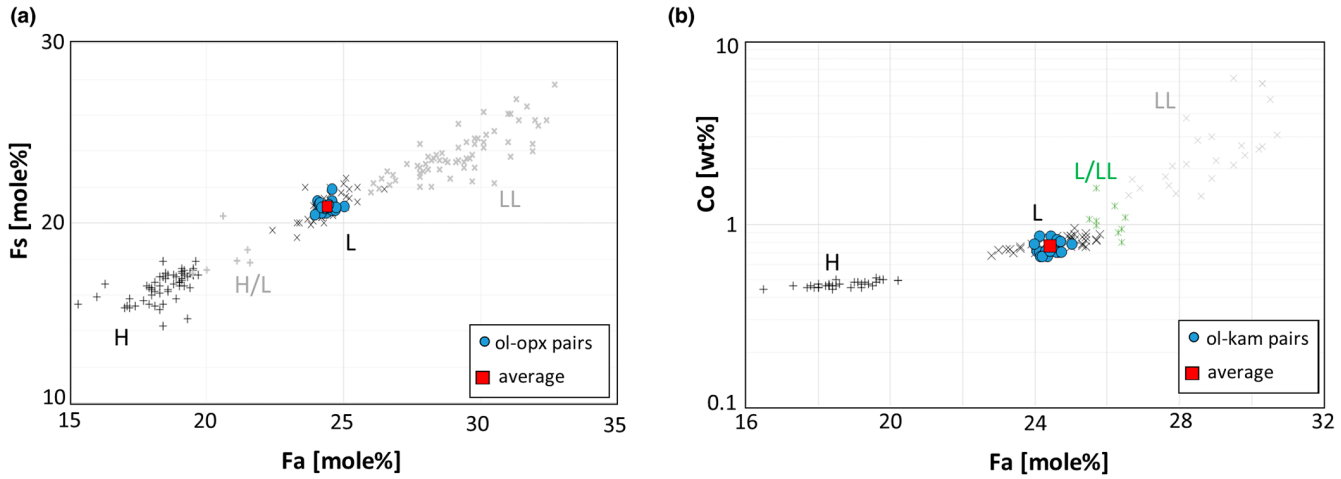

Fig. 12. Composition of olivine, low-Ca pyroxene, and kamacite in Antonin meteorite plots in comparison to compositions of equilibrated ordinary chondrites of H, L, L/LL, and LL groups (data from Brearley & Jones, 1998; Rubin, 1990). a) Fa in olivine versus Fs in low-Ca pyroxene. b) Fa in olivine versus Co in kamacite. In both graphs, analyses of Antonin meteorite cluster well in the field of L chondrites. (Color figure can be viewed at wileyonlinelibrary.com.)

present and well-delineated chondrules are retained. Such local features would suggest petrologic type L4, despite chemical equilibrium of mineral compositions. In the sample examined by us, no signs of brecciation are seen, but Bischoff et al. (2022) suggest that Antonin, as studied in their thin sections, is a nonclastic breccia with L4 and L5 type of material present.

Reconstruction of Shock Processes and Parent Body Evolution

Based on intracrystalline deformation of silicates, manifested by undulose extinction of light by olivine, the shock index can be assigned as moderate, S3 (Stöffler et al., 1991). However, the exact shock history of the sample is plausibly more complex. Very abundant traces of local melting of metal–troilite and plagioclase, formation of chromite–plagioclase assemblages, and plessitic intergrowths of metal, all suggest that the meteorite must have experienced a more severe shock episode in its evolution (Bennett & McSween, 1996; Tomkins, 2009; Tomkins et al., 2013). Plausibly, it experienced a post-shock annealing episode followed by a "secondary" shock event, as suggested for many ordinary chondrites (Rubin, 2004; Ruzicka et al., 2015). Similar features were observed, for example, in LL chondrite MIL 99301 (Rubin, 2002) or H chondrites, for instance Kernouvé (Ruzicka et al., 2015) and Pułtusk (Krzesińska, 2016, 2017) and are generally accepted to be formed in response to shock and post-shock annealing. It is, however, also likely that the Antonin responded very heterogeneously to shock wave, resulting in uneven record of peak shock pressures experienced. This alternative would be in agreement with observations of Bischoff et al. (2022), who studied another part of Antonin sample and concluded it is an S4 chondrite. Whether Antonin records post-shock annealing and "secondary" shock or is highly heterogeneously deformed cannot be concluded with our data and needs further study.

A peculiar feature of Antonin is the presence of mackinawite–troilite assemblages. Sulfides containing Ni are rare in ordinary chondrites (Rubin, 1997) and to our knowledge can be found in LL chondrites, including Chelyabinsk, Appley Bridge, Saint-Severin, and NWA 4859 (Jamsja & Ruzicka, 2010; Schrader & Zega, 2019), but are extremely rare in other groups of ordinary chondrites. We suggest that in Antonin, they formed in response to shock melting and prolonged post-shock annealing. Shock melting of Fe,Ni-metal and troilite would lead to locally restricted formation of homogenous Fe,Ni, S-melt, that under static cooling would separate to kamacite, Ni-poor sulfide, and Ni-rich sulfide phases. Of note is that mackinawite contains less sulfur than troilite, which may indicate shock-induced loss of volatile sulfur that enhanced formation of mackinawite in post-shock conditions. Such interpretation would align with the presence of porous (vaporized) troilite abundantly present in bulk sample. Such shock-induced loss of sulfur would affect Fe-Ni to S ratio, and therefore may favor the formation of S-deficient sulfides during post-shock annealing and cooling. A similar mechanism of sulfur-loss-induced reconstruction of mineralogy in ordinary chondrites was suggested for the formation of native copper grains (Tomkins, 2009). It is our favored interpretation, but other mechanisms remain possible. Sulfides are sensitive to oxygen and sulfur fugacity changes

and therefore may form under significant range of conditions (Schrader & Zega, 2019), which cover melting or phase separation during post-shock conditions (Jamsja & Ruzicka, 2010), but also slow cooling during accretional thermal metamorphism in deep parts of the parent body asteroid (Schrader & Zega, 2019). Further investigations are needed to verify exact formation mechanisms of sulfides in Antonin, but regardless of the exact mechanism, the presence of mackinawite implies an unusual thermal history on the parent body of the meteorite.

Antonin bears record of unusual thermal history on the parent body and also complex shock evolution, involving either multiple impacts and shock annealing or heterogeneous response to shock wave. We suggest that both thermal history and shock evolution can be accounted for if thermal imprint during post-shock thermal episode is taken into account. We hypothesize that lack of textural maturity (retained chondrules and feldspathic fine-grained or glassy material) and simultaneously homogeneous well-equilibrated chemical composition of minerals relate to episodes of shock and post-shock annealing that influenced thermal equilibration of this chondrite. Such a scenario can also explain why parts of Antonin host metal-rich vein-like structures with chondrules retained in the metal and protected from recrystallization (Bischoff et al., 2022). The exact mechanism behind textural inconsistencies, however, cannot be further discussed with our data and more detailed evidence is needed.

As such, Antonin meteorite should be linked to a parent body such as parent bodies of L chondrites. However, it reveals some unusual properties that most plausibly relate to thermal and shock history of the parent asteroid or meteoroid which Antonin was derived from.

Terrestrial Age of Meteorite

Traces of cosmogenic radionuclides ^{48}V and ^{51}Cr detected in Antonin meteorite during gamma spectrometry measurement and having half-life decay time in range of 15–28 days clearly indicate the connection of recovered specimen with a fireball-related fall event. Despite high uncertainty of measurement, the match is evident. Additionally, ^{58}Co, ^{56}Co, ^{46}Sc, ^{57}Co, and ^{54}Mn having decay time in range of a few months, were present in the sample in high concentrations, and measured with uncertainty of 4–6%, which confirms a recent fall of the specimen.

Approximation of Meteoroid Pre-Atmospheric Size

The gamma spectrometry results show the low concentration of ^{26}Al. Formation of this nuclide in meteoroids is strongly affected by shielding conditions, and therefore, concentrations of ^{26}Al in Antonin may indicate one of the three scenarios: (a) origin from an enormous meteoroid chunk, (b) a short cosmic-ray exposure (CRE) time (before the saturation), or (c) the shallow depth of origin of the specimen within the meteoroid. To interpret it, we take into account the ^{60}Co content that is slightly higher in Antonin than in L chondrites with meteoroid radius less than 20 cm (Alexeev et al., 2012), implying Antonin must have been derived from a meteoroid with a size greater than 20 cm.

Combined interpretation of ^{26}Al and ^{60}Co suggests, however, that a meteoroid had a radius lower than 50 cm, plausibly even less than 25 cm, depending on the model applied (Alexeev et al., 2012; Eberhardt et al., 1963; Spergel et al., 1982, 1986). This implies that Antonin did not originate from a large meteoroid chunk, meaning that scenario (a) can be excluded from discussion. The ratio of ^{22}Na/^{26}Al in meteorite, which is, in general, independent of shielding conditions shows also standard value (1.59), and thus, no complex CRE history is suggested. Indeed, complex CRE evolution would be unlikely for a meteoroid 20–50 cm in size. The standard value of ^{22}Na/^{26}Al ratio suggests that short CRE, which is scenario (b) above, can be excluded as well. This implies that Antonin was exposed to cosmic radiation because it was located at a shallow depth, or simply because it originates from a small meteoroid.

L5 and L6 Chondrites with Known Orbits

Comparison of heliocentric orbits of L5 and L6 chondrites with already published parameters is presented in Table 8. We decided to directly compare the size and shape of the orbit and its inclination and not to do a complicated comparison of all orbital parameters and their orbital evolution. In fact, there is not even a large enough number of good quality data to do that. Therefore, we only use the known values of *a*, *e*, and *i* to compare these orbits. However, the Osceola meteorite (Meier et al., 2020) was not included because not enough good data were available to determine the atmospheric trajectory, and thus, the orbit determined is questionable. The orbital parameters for Osceola are (*a, e, i*) = (1.486 AU, 0.3406, 13.20°); errors are unknown. This orbit is not exceptional and the parameters are within the range of other published orbits of L chondrites. The second questionable orbit is that of Ozerki, where both the radiant and the velocity have large errors. Despite this, we kept Ozerki for comparison because the orbit has small value of semimajor axis and eccentricity and some petrographic features of Ozerki indicate possible origin in common with Antonin.

It has been proposed that shocked L chondrites formed during the formation of the Gefion asteroid

Table 8. Comparison of L5 and L6 chondrites with known heliocentric orbits.

Name	Date of fall	Classification	Semimajor axis (AU)	Eccentricity	Inclination (°)	References
Ozerki	2018-06-21	L6, S4/5	0.84 ± 0.02	0.20 ± 0.03	18 ± 3	Kartashova et al. (2020), Gattacceca et al. (2020)
Madura Cave	2020-06-19	L5	0.889 ± 0.003	0.327 ± 0.009	0.12 ± 0.08	Devillepoix et al. (2022)
Antonin	2021-07-15	L5, S3	1.1270 ± 0.0007	0.2285 ± 0.0006	24.22 ± 0.05	This work
Creston	2015-10-24	L5/6, S4	1.300 ± 0.019	0.410 ± 0.013	4.23 ± 0.07	Jenniskens et al. (2019)
Novo Mesto	2020-02-28	L5, S5 breccia	1.451 ± 0.004	0.6087 ± 0.0006	8.76 ± 0.06	Vida et al. (2021), Gattacceca et al. (2021)
Renchen	2018-07-10	L5/6, S4 breccia	1.487 ± 0.005	0.3597 ± 0.0020	23.99 ± 0.07	Spurný et al. (2019), Bischoff et al. (2019)
Jesenice	2009-04-09	L6, S3	1.75 ± 0.07	0.431 ± 0.022	9.6 ± 0.5	Spurný et al. (2010), Bischoff et al. (2011)
Cavezzo	2020-01-01	L5-an, S1 and S3	1.82 ± 0.22	0.46 ± 0.06	4.0 ± 1.6	Gardiol et al. (2021), Pratesi et al. (2021)
Innisfree	1977-02-06	L5 breccia	1.872	0.4732	12.28	Halliday et al. (1978), Kallemeyn et al. (1989)
Novato	2012-10-17	L6, S4 breccia	2.09 ± 0.11	0.526 ± 0.024	5.5 ± 0.6	Jenniskens et al. (2014)
Villalbeto de la Peña	2004-01-04	L6, S4 polymict breccia	2.3 ± 0.2	0.63 ± 0.04	0.0 ± 0.2	Trigo-Rodríguez et al. (2006), Bischoff et al. (2013)
Park Forest	2003-03-27	L5, S5 breccia	2.53 ± 0.19	0.680 ± 0.023	3.2 ± 0.3	Brown et al. (2004), Simon et al. (2004)

Inclinations of orbits are given in the J2000.0.

family located near the 5:2 mean-motion resonance with Jupiter in the middle main belt (Nesvorný et al., 2009). After the fall of the Creston meteorite and the determination of its orbit and the CRE age, however, Jenniskens et al. (2019) studied properties and sources of these meteorites and concluded that there is another source of L chondrites, namely in the inner part of the main belt, from where the meteoroids are transported to the Earth via the ν_6 resonance. Jenniskens et al. (2019) also concluded that L chondrites with small semimajor axis orbits ($a < 2$ AU) came from different collision events, perhaps from the same inner belt source. Additionally, Jenniskens et al. (2019) suggested a completely different source for the Villalbeto de la Peña meteorite than the Gefion family on the basis that it has significantly different mineral composition and contains a winonaite-related fragment in a hydrothermally metamorphosed polymict L-chondritic breccia (Bischoff et al., 2013). We suggest that Antonin originates from a separate body as well, based on orbital parameters of meteoroid, and petrographic features and shock history of meteorite.

Antonin L5 chondrite has the highest value of inclination (however, comparable with Renchen) and one of the smallest values of semimajor axis and eccentricity among known L5 and L6 chondrites. The majority of L chondrites came from orbit with inclination smaller than 10°, and only Antonin, Renchen, and Ozerki (note large error of inclination) have inclination significantly larger than 10°. All these meteorites came from evolved orbits with small semimajor axis and small eccentricity. Antonin and Ozerki have the lowest values of eccentricity of approximately 0.2. This makes these two orbits similar, since no other L chondrite orbit has eccentricity smaller than 0.3, but composition and shock damage of these two meteorites are different. The orbits of Antonin and Renchen are also very similar, mainly due to the high value of orbital inclination. Moreover, both orbits are equally oriented in the solar system. In fact, the orbit of Antonin is most similar to the orbits of the LL7 chondrite Dishchii'bikoh with (a, e, i) = (1.13 AU, 0.21, 21.2°) (Jenniskens et al., 2020; Palotai et al., 2019) and the H4 chondrite Buzzard Coulee with (a, e, i) = (1.23 AU, 0.22, 25.5°) (Brown et al., 2011; Milley, 2010). This demonstrates that there is no direct relation between chondrite type and orbit.

The known orbits of L chondrites show that the semimajor axis can take values ranging from 2.5 to 0.8 AU and eccentricities from 0.7 to 0.2. The inclination is usually less than 10° and rarely reaches a value around 20°; the orbit has then both small semimajor axis and eccentricity. Based on the diversity of L chondrite orbits, we confirm the result of Jenniskens et al. (2019) that there are multiple sources and collision events of L5 and L6 chondrites. The Antonin meteorite probably does not originate from the

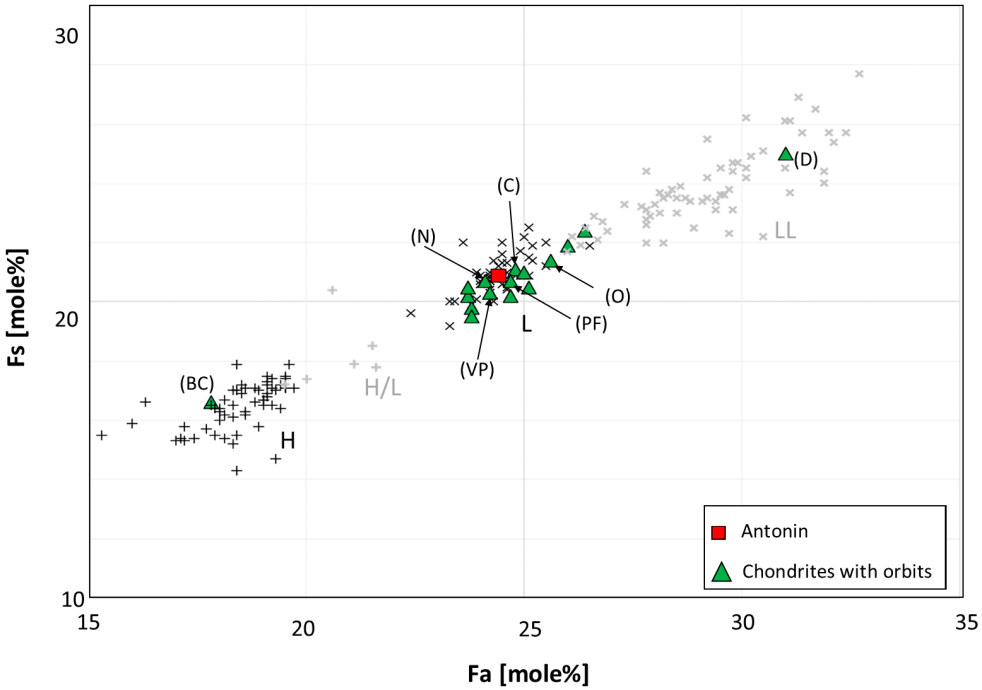

Fig. 13. Composition of Antonin and other L chondrites with known orbits as well as Buzzard Coulle (BC; H4 ordinary chondrite) and Dishchii'bikoh (D; LL7 ordinary chondrite) which have similar orbital parameters to Antonin. L chondrites, close in Fa-Fs composition to Antonin and showing petrographic similarities are marked by arrows: Villalbeto de la Peña (VP), Novato (N), Park Forest (PF), Creston (C), and Ozerki (O). Data on L chondrites from Meteoritical Bulletin database. (Color figure can be viewed at wileyonlinelibrary.com.)

Gefion asteroid family but from a source in the inner main belt.

Composition of olivine and low-Ca pyroxene of Antonin falls well in the middle of the L chondrite field. For comparison, data for all L chondrites with known orbits are plotted in Fig. 13 and no obvious compositional match appears from this scatter. The closest compositional match to Antonin is shown for Novato (L6), Villalbeto de la Peña (L6), Park Forest (L5), and Creston (L6), but most likely none of the matches have parent body implications, as petrographically these meteorites are highly different than Antonin. In contrast, petrographic similarities exist for Antonin and Ozerki (L6) chondrite, despite significant difference of olivine and pyroxene compositions of the two (Fig. 13). Antonin contains porous troilite and mackinawite–troilite assemblages (Fig. 10c), which are rare in ordinary chondrites (detailed discussion in section Reconstruction of Shock Processes and Parent Body Evolution) and plausibly formed in response to complex shock and thermal evolution of the parent body. In this aspect, Antonin is unlike typical L chondrites. However, the presence of Ni-rich sulfides, pentlandite with 15.4 wt% Ni and heazlewoodite with up to 71.5 wt% Ni, was reported for the Ozerki L6 chondrite (Gattacceca et al., 2020). The fact that Ozerki contains porous troilite and mosaic Ni-bearing sulfides suggests similarities to Antonin shock history with intense localized shock melting and vaporization of S. The two meteorites, however, must have undergone different oxidation processes, which is reflected in the differences of olivine and pyroxene Fe contents (Fig. 13). This implies that no simple connection can be made for Antonin and other L chondrites with known orbits.

CONCLUSIONS

- Majority of atmospheric trajectory and heliocentric orbit of daylight fireball were determined on the basis of three video records from cameras of the Czech part of the EN. On August 3, 2021, one piece of meteorite of 350 g of mass was recovered on the basis of these data and subsequently named Antonin.
- The specimen was, immediately after recovery, analyzed for the presence of short-lived cosmogenic nuclides to verify its fresh nature. Traces of nuclides having half-life in range of a couple of days were detected during analysis and this ultimately confirms connection of the meteorite find with the fireball event.
- The recovered meteorite represents unbrecciated L5 chondrite. It is very well equilibrated chemically,

but less equilibrated texturally. Many chondrules and glassy mesostasis are retained in the sample. Meteorite is weakly–moderately shocked, as revealed by intracrystalline deformation of silicates. However, the meteorite must have experienced quite strong (higher than S3) shock metamorphism in its evolution. It is possible that it experienced shock, post-shock annealing, and next shock event. Alternatively, the shock episode may have affected the rock highly heterogeneously. This is manifested by the presence of plessitic metal aggregates, porous troilite, intergrowths of mackinawite within troilite, and very abundant products of local shock melting such as globular shock melt pockets at the contacts of metal and plagioclase or chromite–plagioclase assemblages.

- The heliocentric orbit of the Antonin bolide has the highest value of inclination and one of the smallest values of semimajor axis and eccentricity among known L5 and L6 chondrites. The meteorite probably originated in the inner asteroid belt.
- Isotopic measurements indicate that Antonin was derived from a meteoroid with pre-atmospheric size greater than 20 cm in radius and initial dynamic mass modeling provided pre-atmospheric radius of the meteoroid of 15–20 cm for the determined density 3.42 g cm^{-3}.
- There is no obvious relationship between Antonin and other recently documented L5 and L6 ordinary chondrite falls. Orbital parameters, petrographic features, and shock history of Antonin suggest that it originated from a different source compared to previously documented falls.

Acknowledgments—We would like to thank Jon M. Friedrich and Matthias M. M. Meier for their helpful reviews and the Associate Editor Josep M. Trigo-Rodríguez. We also thank all the witnesses for their reports on this fireball and Dr. Radmila Brožková from the Czech Hydrometeorological Institute for the high-altitude wind data needed to calculate the meteorite impact area. This work was supported by the institutional project RVO: 67985815, grant no. 19-26232X from the Czech Science Foundation. AMK acknowledges support from Research Council of Norway through its Centres of Excellence funding scheme, project number 223272. Siri Simonsen and Muriel Erambert (UiO) are thanked for assistance in SEM and EPMA data collection. ZT would like to thank Agnieszka Burakowska, who performed gamma-ray spectrometry measurement, and Katarzyna Tymińska and Michal Kuć for numerical modeling and mapping of the measurement object. The access to laboratories was made possible via internal infrastructure of National Centre for Nuclear Research, Poland. Andrzej Owczarzak is thanked for participation in meteorite recovery trip and for his assistance in transferring the type specimen for classification. The authors have no conflict of interest to declare.

Data Availability Statement—Data are available on request from the authors. The data that support the findings of this study are available from the corresponding author upon reasonable request.

Editorial Handling—Dr. Josep M. Trigo-Rodríguez

REFERENCES

Alexeev, V. A., Gorin, V. D., Ivliev, A. I., Kashkarov, L. L., Ott, U., Sadilenko, D. A., and Ustinova, G. K. 2012. Integrated Study of the Thermoluminescence, Noble Gases, Tracks, and Radionuclides in the Fresh Fallen Ash Creek L6 and Tamdakht H5 Chondrites. *Geochemistry International* 50: 105–24.

Bennett, M. E., and McSween, H. Y. 1996. Shock Features in Iron-Nickel Metal and Troilite of L-Group Ordinary Chondrites. *Meteoritics & Planetary Science* 31: 255–64.

Bischoff, A., Barrat Jean, A., Berndt, J., Borovička, J., Burkhardt, C., Busemann, H., Hakenmüller, J., et al. 2019. The Renchen L5-6 Chondrite Breccia – The First Confirmed Meteorite Fall from Baden-Württemberg (Germany). *Geochemistry* 79: 125525.

Bischoff, A., Dyl, K. A., Horstmann, M., Ziegler, K., Wimmer, K., and Young, E. D. 2013. Reclassification of Villalbeto de la Peña—Occurrence of a Winonaite-Related Fragment in a Hydrothermally Metamorphosed Polymict L-Chondritic Breccia. *Meteoritics & Planetary Science* 48: 628–40.

Bischoff, A., Jersek, M., Grau, T., Mirtic, B., Ott, U., Kučera, J., Horstmann, M., et al. 2011. Jesenice—A New Meteorite Fall from Slovenia. *Meteoritics & Planetary Science* 46: 793–804.

Bischoff, A., Patzek, M., Peters, S. T. M., Barrat, J.-A., Di Rocco, T., Pack, A., Ebert, S., Jansen, C. A., and Kmieciak, K. 2022. The Chondrite Breccia of Antonin (L4-5)—A New Meteorite Fall from Poland with a Heterogeneous Distribution of Metal. *Meteoritics & Planetary Science*. https://doi.org/10.1111/maps.13905.

Borovička, J., Bettonvil, F., Baumgarten, G., Strunk, J., Hankey, M., Spurný, P., and Heinlein, D. 2021. Trajectory and Orbit of the Unique Carbonaceous Meteorite Flensburg. *Meteoritics & Planetary Science* 56: 425–39.

Borovička, J., Spurný, P., and Shrbený, L. 2019. New Spectroscopic Program of the European Fireball Network. Proceedings, International Meteor Conference. pp. 28–32.

Borovička, J., Spurný, P., and Shrbený, L. 2020. Two Strengths of Ordinary Chondritic Meteoroids as Derived from Their Atmospheric Fragmentation Modeling. *The Astronomical Journal* 160: 42.

Borovička, J., Spurný, P., Shrbený, L., Štork, R., Kotková, L., Fuchs, J., Keclíková, J., et al. 2022. Data on 824 Fireballs Observed by the Digital Cameras of the European Fireball Network in 2017–2018 I. Description

of the Network, Data Analysis, and the Catalog. *Astronomy and Astrophysics* 667: A157.
Brearley, A. J., and Jones, R. H. 1998. Chondritic Meteorites. In *Planetary Materials*, edited by J. J. Papike, 3-1–3-398. Washington, D.C.: Mineralogical Society of America.
Brown, P., McCausland, P. J. A., Fries, M., Silber, E., Edwards, W. N., Wong, D. K., Weryk, R. J., Fries, J., and Krzeminski, Z. 2011. The Fall of the Grimsby Meteorite—I: Fireball Dynamics and Orbit from Radar, Video, and Infrasound Records. *Meteoritics & Planetary Science* 46: 339–63.
Brown, P., Pack, D., Edwards, W. N., Revelle, D. O., Yoo, B. B., Spalding, R. E., and Tagliaferri, E. 2004. The Orbit, Atmospheric Dynamics, and Initial Mass of the Park Forest Meteorite. *Meteoritics & Planetary Science* 39: 1781–96.
Ceplecha, Z. 1987. Geometric, Dynamic, Orbital and Photometric Data on Meteoroids from Photographic Fireball Networks. *Bulletin of the Astronomical Institute of Czechoslovakia* 38: 222–34.
Colas, F., Zanda, B., Bouley, S., Jeanne, S., Malgoyre, A., Birlan, M., Blanpain, C., et al. 2020. FRIPON: A Worldwide Network to Track Incoming Meteoroids. *Astronomy and Astrophysics* 644: A53.
Devillepoix, H. A. R., Sansom, E. K., Shober, P., Anderson, S. L., Towner, M. C., Lagain, A., Cupák, M., et al. 2022. Trajectory, Recovery, and Orbital History of the Madura Cave Meteorite. *Meteoritics & Planetary Science* 57: 1328–38. https://doi.org/10.1111/maps.13820.
Eberhardt, P., Geiss, J., and Lutz, H. 1963. Neutrons in meteorites. In *Earth Science and Meteoritics*, edited by J. Geiss and E. D. Goldberg, 143–68. Amsterdam: North-Holland Publ. Co.
Gardiol, D., Barghini, D., Buzzoni, A., Carbognani, A., Di Carlo, M., Di Martino, M., Knapic, C., et al. 2021. Cavezzo, the First Italian Meteorite Recovered by the PRISMA Fireball Network. Orbit, Trajectory, and Strewn-Field. *Monthly Notices of the Royal Astronomical Society* 501: 1215–27.
Gattacceca, J., McCubbin, F. M., Bouvier, A., and Grossman, J. 2020. The Meteoritical Bulletin, No. 107. *Meteoritics & Planetary Science* 55: 460–2.
Gattacceca, J., McCubbin, F. M., Grossman, J., Bouvier, A., Bullock, E., Chennaoui, A. H., Debaille, V., et al. 2021. The Meteoritical Bulletin, No. 109. *Meteoritics & Planetary Science* 56: 1626–30.
Halliday, I., Blackwell, A. T., and Griffin, A. A. 1978. The Innisfree Meteorite and the Canadian Camera Network. *Journal of the Royal Astronomical Society of Canada* 72: 15–39.
Hankey, M., Perlerin, V., and Meisel, D. 2020. The All-Sky-6 and the Video Meteor Archive System of the AMS Ltd. *Planetary and Space Science* 190: 105005.
Hutchison, R. 2004. *Meteorites: A Petrologic Chemical and Isotopic Synthesis*. Cambridge: Cambridge University Press.
Jamsja, N., and Ruzicka, A. 2010. Shock and Thermal History of Northwest Africa 4859, an Annealed Impact-Melt Breccia of LL Chondrite Parentage Containing Unusual Igneous Features and Pentlandite. *Meteoritics & Planetary Science* 45: 828–49.
Jenniskens, P., Moskovitz, N., Garvie, L. A. J., Qing-Z, Y., Howell, J. A., Free, D. L., Albers, J., et al. 2020. Orbit and Origin of the LL7 Chondrite Dishchii'bikoh (Arizona). *Meteoritics & Planetary Science* 55: 535–57.
Jenniskens, P., Rubin, A. E., Yin, Q., Sears, D. W. G., Sandford, S. A., Zolensky, M. E., Krot, A. N., et al. 2014. Fall Recovery and Characterization of the Novato L6 Chondrite Breccia. *Meteoritics & Planetary Science* 49: 1388–425.
Jenniskens, P., Utas, J., Yin, Q.-Z., Matson, R. D., Fries, M., Howell, J. A., Free, D., et al. 2019. The Creston, California, Meteorite Fall and the Origin of L Chondrites. *Meteoritics & Planetary Science* 54: 699–720.
Kalasová, D., Zikmund, T., Spurný, P., Haloda, J., Borovička, J., and Kaiser, J. 2020. Chemical and Physical Properties of Žďár Nad Sázavou L Chondrite and Porosity Differentiation Using Computed Tomography. *Meteoritics & Planetary Science* 55: 1073–81.
Kallemeyn, G. W., Rubin, A. E., Wang, D., and Wasson, J. T. 1989. Ordinary Chondrites: Bulk Compositions Classification Lithophile-Element Fractionations and Composition-Petrographic Type Relationships. *Geochimica et Cosmochimica Acta* 53: 2747–67.
Kartashova, A., Golubaev, A., Mozgova, A., Chuvashov, I., Bolgova, G., Glazachev, D., and Efremov, V. 2020. Investigation of the Ozerki meteoroid parameters. *Planetary and Space Science* 193: A105034.
Krzesińska, A. M. 2016. Thermal Metamorphic Evolution of the Pułtusk H Chondrite Breccia – Compositional and Textural Properties Not Included in Petrological Classification. *Geological Quarterly* 60: 211–24.
Krzesińska, A. M. 2017. Contribution of Early Impact Events to Metal-Silicate Separation Thermal Annealing and Volatile Redistribution: Evidence in the Pułtusk H Chondrite. *Meteoritics & Planetary Science* 52: 2305–21.
Laubenstein, M., Giampaoli, A., Janowski, P., and Mietelski, J. W. 2012. Cosmogenic Radionuclides in the Sołtmany L6 Meteorite. *Meteorites* 2: 45–51.
Meier, M. M. M., Gritsevich, M. Welten, K. C., Lyytinen, E., Plant, A. A., Maden, C., and Busemann, H. 2020. Orbit, Meteoroid Size and Cosmic History of the Osceola (L6) Meteorite. 14th Europlanet Science Congress 2020, Id. EPSC2020-730.
Milley, E. P. 2010. Physical Properties of Fireball-Producing Earth-Impacting Meteoroids and Orbit Determination through Shadow Calibration of the Buzzard Coulee Meteorite Fall. PhD thesis, University of Calgary, Calgary, Alberta, Canada.
Nesvorný, D., Vokrouhlický, D., Morbidelli, A., and Bottke, W. F. 2009. Asteroidal Source of L Chondrite Meteorites. *Icarus* 200: 698–701.
Owczarzak, A. 2021. New Decline in Poland. *Meteoryt* 101: 15.
Palotai, C., Sankar, R., Free, D. L., Howell, J. A., Botella, E., and Batcheldor, D. 2019. Analysis of the 2016 June 2 Bolide Event over Arizona. *Monthly Notices of the Royal Astronomical Society* 487: 2307–18.
Pouchou, J. L., and Pichoir, F. 1991. Quantitative Analysis of Homogeneous or Stratified Microvolumes Applying the Model "PAP." In *Electron Probe Quantification*, edited by K. F. J. Heinrich and D. E. Newbury, 31–75. New York: Plenum Press.
Povinec, P., Masarik, J., Sýkora, I., Kováčik, A., Beňo, J., Meier, M. M. M., Wieler, R., Laubenstein, M., and Porubčan, V. 2015. Cosmogenic Nuclides in the Košice Meteorite: Experimental Investigations and Monte Carlo Simulations. *Meteoritics & Planetary Science* 50: 880–92.
Pratesi, G., Moggi, C. V., Greenwood, R. C., Franchi, I. A., Hammond, S. J., Di Martino, M., Barghini, D., et al.

2021. Cavezzo-the Double Face of a Meteorite: Mineralogy Petrography and Geochemistry of a Very Unusual Chondrite. *Meteoritics & Planetary Science* 56: 1125–50.

Revelle, D. O., and Ceplecha, Z. 2001. Bolide Physical Theory with Application to PN and EN Fireballs. Proceedings, Meteoroids 2001 Conference, pp. 507–512.

Rubin, A. E. 1990. Kamacite and Olivine in Ordinary Chondrites: Intergroup and Intragroup Relationships. *Geochimica et Cosmochimica Acta* 54: 1217–32.

Rubin, A. E. 1997. Mineralogy of Meteorite Groups. *Meteoritics & Planetary Science* 32: 231–47.

Rubin, A. E. 2002. Post-Shock Annealing of Miller Range 99301 (LL6): Implications for Impact Heating of Ordinary Chondrites. *Geochimica et Cosmochimica Acta* 66: 3327–37.

Rubin, A. E. 2004. Postshock Annealing and Postannealing Shock in Equilibrated Ordinary Chondrites: Implications for the Thermal and Shock Histories of Chondritic Asteroids. *Geochimica et Cosmochimica Acta* 68: 673–89.

Ruzicka, A., Hugo, R., and Hutson, M. 2015. Deformation and Thermal Histories of Ordinary Chondrites: Evidence for Post-Deformation Annealing and Syn-Metamorphic Shock. *Geochimica et Cosmochimica Acta* 163: 219–33.

Schneider, C. A., Rasband, W. S., and Eliceiri, K. W. 2012. NIH Image to ImageJ: 25 Years of Image Analysis. *Nature Methods* 9: 671–5.

Schrader, D. L., and Zega, T. J. 2019. Petrographic and Compositional Indicators of Formation and Alteration Conditions from LL Chondrite Sulphides. *Geochimica et Cosmochimica Acta* 264: 165–79.

Shrbený, L., Spurný, P., and Borovička, J. 2020. Fireball Fragmentation in the First Half of the Atmospheric Trajectory. *Planetary and Space Science* 187: 104956.

Simon, S. B., Grossman, L., Clayton, R. N., Mayeda, T. K., Schwade, J. R., Sipiera, P. P., Wacker, J. F., and Wadhwa, M. 2004. The Fall Recovery and Classification of the Park Forest Meteorite. *Meteoritics & Planetary Science* 39: 625–34.

Spergel, M. S., Reedy, R. C., Lazareth, O. W., and Levy, P. W. 1982. Cosmic-Ray COBALT-60 in Chondrites. *Lunar and Planetary Science XIII*, pp. 756–7. Abstract.

Spergel, M. S., Reedy, R. C., Lazareth, O. W., Levy, P. W., and Slatest, L. A. 1986. Cosmogenic Neutron-Capture-Produced Nuclides in Stony Meteorites. *Journal of Geophysical Research* 91: D483–94.

Spurný, P., Borovička, J., Kac, J., Kalenda, P., Atanackov, J., Kladnik, G., Heinlein, D., and Grau, T. 2010. Analysis of Instrumental Observations of the Jesenice Meteorite Fall on April 9, 2009. *Meteoritics & Planetary Science* 45: 1392–407.

Spurný, P., Borovička, J., Mucke, H., and Svoreň, J. 2017. Discovery of a New Branch of the Taurid Meteoroid Stream as a Real Source of Potentially Hazardous Bodies. *Astronomy and Astrophysics* 605: A68.

Spurný, P., Borovička, J., and Shrbený, L. 2020. The Žďár Nad Sázavou Meteorite Fall: Fireball Trajectory Photometry Dynamics Fragmentation Orbit and Meteorite Recovery. *Meteoritics & Planetary Science* 55: 376–401.

Spurný, P., Borovička, J., Shrbený, L., Ronge, L., and Heinlein, D. 2019. The Hradec Králové (CZ) and Renchen (DE) Meteorite Falls—Recovery of Meteorites Exactly According to Prediction Based on Records Taken by the European Fireball Network. Oral Presentation at Meteoroids 2019, Bratislava, Slovakia.

Stöffler, D., Keil, K., and Scott, E. R. D. 1991. Shock Metamorphism in Ordinary Chondrites. *Geochmica et Cosmochimica Acta* 55: 3845–67.

Tomkins, A. G. 2009. What Metal-Troilite Textures Can Tell us about Post-Impact Metamorphism in Chondrite Meteorites. *Meteoritics & Planetary Science* 44: 1133–49.

Tomkins, A. G., Weinberg, R. F., Schaefer, B. F., and Lagendam, A. 2013. Disequilibrium Melting and Melt Migration Driven by Impacts: Implications for Rapid Planetesimal Core Formation. *Geochimica et Cosmochimica Acta* 100: 41–59.

Trigo-Rodríguez, J. M., Borovička, J., Spurný, P., Ortiz, J. L., Docobo, J. A., Castro-Tirado, A. J., and Llorca, J. 2006. The Villalbeto de la Peña Meteorite Fall: II. Determination of Atmospheric Trajectory and Orbit. *Meteoritics & Planetary Science* 41: 505–17.

Tymiński, Z., Hult, M., Krzesińska, A. M., Tymińska, K., Lutter, G., Saganowski, P., Marissens, G., et al. 2022. Underground Radioactivity Measurements of Meteorites: Development of Methods Suitable to Determine Precise Terrestrial Age of Recent Falls (in review).

Vida, D., Šegon, D., Šegon, M., Atanackov, J., Ambrožič, B., McFadden, L., Ferrière, L., et al. 2021. Novo Mesto Meteorite Fall—Trajectory, Orbit, and Fragmentation Analysis from Optical Observations. 15th Europlanet Science Congress 2021, EPSC2021-139.

Wilkinson, S. L., and Robinson, M. S. 2000. Bulk Density of Ordinary Chondrite Meteorites and Implications for Asteroidal Internal Structure. *Meteoritics & Planetary Science* 35: 1203–13.